ELSEVIER

Journal of Power Sources 67 (1997) 257–265

JOURNAL OF POWER SOURCES

Improved lead alloys for lead/acid positive grids in electric-vehicle applications

L. Albert [a,*], A. Chabrol [b], L. Torcheux [b], Ph. Steyer [c], J.P. Hilger [c]

[a] *Metaleurop Recherche, 1 avenue A. Einstein, BP 120, 78193 Trappes, France*
[b] *Exide Europe, CEAC, 5–7 allée des Pierres Mayettes, 92636 Gennevilliers, France*
[c] *Laboratoire du Solide Minéral, CNRS URA 158, Université H. Poincaré Nancy I, BP 239, 54506 Vandoeuvre-les-Nancy, France*

Received 11 September 1996; accepted 30 December 1996

Abstract

Currently, the excessive weight of the positive grid is a limiting factor to the increase of the specific energy of the lead/acid battery. With present alloys, a thickness of a few millimeters is a pre-requisite in the processing of a positive grid which is submitted to heavy corrosion during the charge and deep-discharge cycles usually encountered with electric vehicles. The search for a lighter battery approaching the ALABC's goal of 50 Wh kg^{-1} therefore requires the development of a new set of alloys that are able to withstand mechanical stress and corrosion experienced by a positive grid during the service life of an electric-vehicle battery. The work reported here shows that tin addition (to a level of 1.2 wt.%) or combined tin (to a level of 0.6 wt.%) and silver (to a level of 0.05 wt.%) additions increase considerably both the mechanical properties and the corrosion resistance of a Pb–0.08wt.%Ca–0.013wt.%Al alloy. Gravity casting trials reveal that the tin-rich alloy (1.2 wt.%) and the silver-rich alloy (0.05 wt.%) could be used directly in the industrial processing of batteries that use gel technology. Information is also given on the performances of these batteries when submitted to the international TC69 cycling test, as well as indications of the minimum grid thickness that could be achieved with these alloys without sacrificing battery cycle life. © 1997 Elsevier Science S.A.

Keywords: Lead/acid batteries; Corrosion; Passivation; Alloys; Electric vehicles; Lead; Calcium; Tin; Silver

1. Introduction

The development of lead/acid batteries for electric vehicle (EV) applications requires the definition of specific alloys for the positive grids that are able to sustain the intensive stress and corrosion that occur in the positive plates during cycling. The work reported here concerns experiments carried out for the definition of a Pb–Ca–Sn–Ag alloy that: (i) is less sensitive to passivation; (ii) has an improved resistance to corrosion, and (iii) has improved mechanical properties.

This alloy should enable the processing of thinner positive grids with an equivalent service life.

The effect of tin addition (up to the level of 1.2 wt.%) or silver addition (up to the level of 0.1 wt.%) to a Pb–0.08wt.%Ca–0.6wt.%Sn reference alloy have been investigated in the laboratory and then used in the processing of fully operative batteries which have been tested under cycling conditions.

2. Experimental

2.1. Grid casting

Grids from a reference alloy (Pb–0.08wt.%Ca–0.6wt.%Sn–0.013wt.%Al), a tin-rich alloy (Pb–0.08wt.%Ca–1.2wt.%Sn–0.013wt.%Al) and two silver-rich alloys (Pb–0.08wt.%Ca–0.6wt.%Sn–0.013wt.%Al with, respectively, 0.05 and 0.1 wt.% of Ag) (see Table 1) were produced on a standard book-mould Wirtz machine at a casting rate of 13 double panels per min. The alloy was held at 470 °C before being poured, via a ladle, into the mould, held at a temperature of around 150 °C. The grids were left to cool at room temperature on the caster grid rack.

The grids (138 g with a 2.65 mm thickness) were used in the processing of 12 V, 55 Ah batteries with a gelled

* Corresponding author.

PII S0378-7753(97)02556-1

Table 1
Alloy composition

Alloy	Ca (ppm)	Sn (wt.%)	Ag (ppm)
Reference	790	0.64	30
Sn-rich	790	1.20	29
Ag-rich I	770	0.64	480
Ag-rich II	750	0.64	1070

electrolyte and a high density paste. Small tetrabasic crystals were obtained upon curing. The active material composition after tank formation was quite similar for all the plates, as given by X-ray diffraction with an INEL–CPS 120 spectrometer and the CSIRO Peaks® software (typical composition: 28 wt.% α-PbO_2, 70 wt.% β-PbO_2, 2 wt.% $PbSO_4$, error = ± 4 wt.%).

In parallel, samples dedicated to laboratory-scale experiments (tensile strength tests, creep resistance test, corrosion resistance tests) were cast at 600 °C in a 3 mm, 200 °C, copper mould to reproduce as closely as possible the high cooling rates experienced by the alloy during the industrial manufacturing of grids. In some cases, for comparative purposes cast samples were rolled from a thickness of 7 to 3 mm with a laboratory rolling mill. An annealing treatment at 310 °C for 2 h was also performed on 3 mm cast samples to evaluate the performance of the alloys after dissolution and rehomogenization of all the precipitated compounds.

2.2. Bare-grid characterization

2.2.1. Mechanical properties

The mechanical properties of the grids were evaluated through statistical creep resistance tests at 27 MPa carried out directly on grid wires (100 wires tested per alloy). The creep resistance of the alloy was estimated by the time that elapsed between the loading of the samples and their rupture. Three criteria were in fact recorded: (i) the average creep-to-failure-time; (ii) the maximum creep-to-failure-time, and (iii) the percentage of wires broken after 20 h. These experiments were completed by more classical tensile strength tests and creep resistance tests (under a loading charge of 20.7 MPa) that were carried out on laboratory samples aged for 72 h at 60 °C to simulate the curing and the formation steps experienced by each alloy during the battery process. In some cases, the alloy Vickers hardness was measured as a function of time.

2.2.2. Corrosion resistance

The corrosion resistance of bare grids was investigated over a polarization period of 13 days in 4.8 M H_2SO_4 at +1500 mV and 50 °C to simulate the end-of-charge of the batteries. All the potentials given in this paper are referred to the mercurous sulfate/mercury reference electrode (Hg/Hg_2SO_4). The corrosion resistance was estimated by the measurement of the amount of corrosion products formed at the metal surface and by the observation of the corrosion profile on a cross section of a grid wire. The amount of corrosion products was obtained by comparison of the grid weights before and after dissolution of the oxides in a CH_3COOH/N_2H_5OH (hydrazinion hydroxide) solution [1]. These data, on bare grids, were completed by some experiments on laboratory samples that were polarized for 5 days in 5 M H_2SO_4, +1500 mV at 50 °C. The corrosion resistance of the samples was determined using the same procedure.

2.2.3. Passivation resistance

The passivation resistance of the grids was evaluated through an experiment [1] that involved passivation of the grids in a 0.3 M H_2SO_4 solution at 700 mV and 25 °C for 18 h and then characterization of the conductivity of the corrosion products by a set of three voltammetric scans (at 1 mV s^{-1}) from +1600 to −1600 mV. It is assumed that, during the first scan, the oxidation current at +1600 mV and the amount of PbO_2 reduced to $PbSO_4$ (determined by the area of the Pb^{II}/Pb^{IV} reduction peak) would depend on the conductivity of the PbO layer formed at the metal surface during the passivation step. It is also concluded that, since at the end of the first cycle all the lead contained in the corrosion products is transformed into a metallic form, these two values will be, during the second and third scans, representative of a perfectly conducting metal/oxide interface and can, therefore be used as references. The passivation degree of the grids is then characterized by two ratios R and C where:

1. R is the ratio (intensity at 1600 mV recorded during the third scan)/(intensity at 1600 mV during the first scan), and
2. C is the ratio (area of the peak corresponding to the transformation $PbO_2/PbSO_4$ during the third scan)/(area of the peak corresponding to the transformation $PbO_2/PbSO_4$ during the first scan).

R and C values close to unity are representative of the formation of a conductive corrosion layer.

These experiments carried out on bare grids were completed by some experiments on the passivation resistance of laboratory samples placed under conditions that simulate a deep-discharge (polarization 7 days in a 0.5 M H_2SO_4 solution at +700 mV). During these experiments, the thickness and the composition of the corrosion products formed at the metal surface were recorded on a cross section of a corroded sample. The different corrosion products were analysed by electron probe micoranalysis (EPMA) (CAMECA SX 50) and scanning electron microscopy (SEM) (HITACHI 2500). The micro-hardness of the lead monoxide layer was measured with a Reiched MeF metallographical microscope.

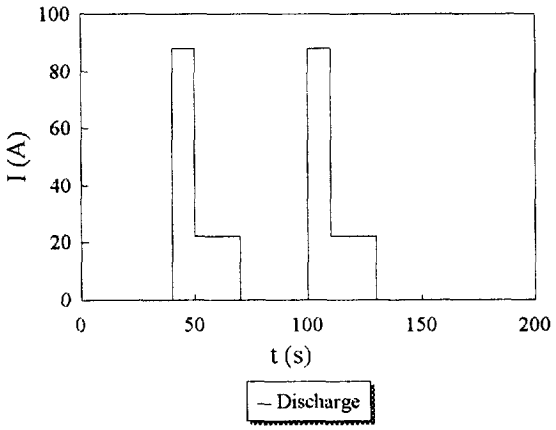

Fig. 1. TC 69 cycling test: discharge current profile vs. time (2 micro-cycles are shown).

2.3. Battery performance evaluation (TC 69 cycling test and self-discharge)

The gel batteries were tested, after training, in accordance with the international TC 69 cycling test. The TC 69 cycling test is a dynamic test that consists of a series of 60 s high-intensity discharge microcycles (Fig. 1) that simulate EV duty. The series of microcycles is repeated until the voltage falls to 8.6 V, i.e., until the depth-of-discharge reaches 100%. This discharge period is followed by a recharge period (three steps at a constant currents of 11, 4 and 0.7 A, respectively, with voltage limitation at 14.4 V followed by a constant-current period of 2.5 h at 0.7 A) which is tuned up to reach an overcharge coefficient of around 1.1. During the cycling test, the battery performance is monitored by conducting $C/5$, $C/20$, $C/5$ capacity tests every 25 cycles. Both the energy recovered during the TC 69 discharge period and the second $C/5$ capacity test were recorded versus the number of cycles.

After cycling, the batteries were weighed and subjected to a tear-down analysis. The latter involved measuring the battery grid growth, grid weight loss and analysis of the negative material by atomic absorption.

In parallel, the self-discharge behaviour was assessed by measuring the voltage and $C/5$ capacity variations during a storage period of 90 days at 25 °C. The initial value was recorded after a conditioning period of five cycles at a 5 h discharge.

3. Results

3.1. Structural and mechanical properties of silver-rich and tin-rich alloys

Immediately after casting, metallographic cuts carried out on the alloys show that all the grids exhibit a large grain structure, oriented in the direction of the predominant heat flow, with 5 to 6 grains in the wire section. If nearly complete discontinuous transformation ('puzzling') can be observed on the reference alloy, the tin-rich alloy keeps its foundry basaltic structure. In the case of the silver-rich alloys, large segregations are observed at the grain boundaries and the dendritic sub-boundaries. SEM investigations suggest that these segregations contain pure aluminum and silver as intermetallics such as Ag_xAl_y and Ag_xSn_y in accordance with the binary phase diagrams.

Upon ageing, the structure and properties of alloys evolve with time. The metallographic cuts carried out on grids after one year at 20 °C show (Fig. 2) that some 'overaged' areas are clearly visible in the reference alloy, while the volume of 'overaged' areas is significantly reduced in the silver-rich II alloy. This result suggests that silver, at a level of 0.1 wt.%, has a delaying effect on the occurrence of the 'overageing' phenomenon.

These observations were confirmed by hardness measurements. Fig. 3 depicts the evolution of the hardness of cast samples versus time during an ageing period at 80 °C. If the decrease in the hardness, associated with the evolution of the structure ('overageing'), is clearly visible on the reference alloy, the stability of the hardness of the alloys enriched with silver is consistent with the hypothesis of an inhibiting effect of silver (at a level of 0.1 wt.%) versus the 'overageing' phenomenon.

It is believed that high mechanical properties, particularly creep resistance, may decrease the tendency for the grid to grow with cycling and prevent battery failure by

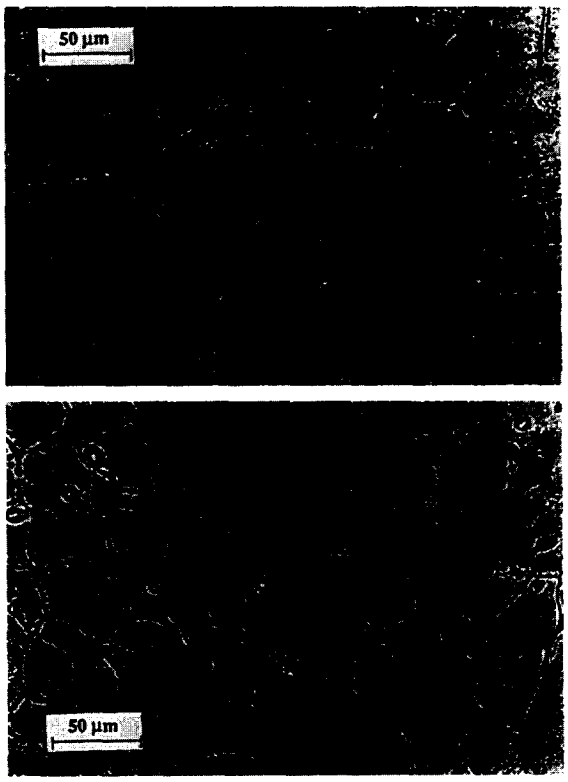

Fig. 2. Metallographic cross sections after one year at 25 °C.

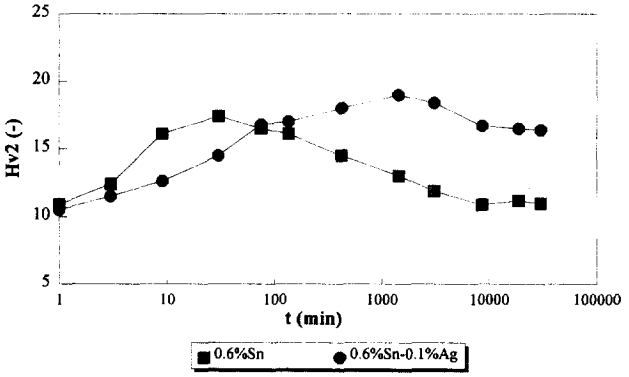

Fig. 3. Hardness evolution vs. time at 20 °C (Pb–0.1wt.%Ca).

short-circuits between the positive grids and the negative compartment [3,11].

Fig. 4 shows the effect of tin or silver additions on the creep resistance, at 27 MPa, of industrial bare-grid wires. The latter is presented by the creep-to-failure-times (average and maximum) and by the number of grid wires broken after 20 h. These data show that the maximum creep resistance increases significantly (from 200 to 500 h) with a tin or a low silver addition. This result also suggests that the silver-rich II alloy may be a source of a problem on cycling since, as seen on Fig. 4, the percentage of grid wires broken after only 20 h is excessively high (around 75%). The latter was confirmed during the industrial processing of the plates: the silver-rich II alloy turned out to be brittle during the pasting and cell assembly operations.

These results are found to be consistent with the experiments carried out on laboratory samples. Figs. 5 and 6 show the effect of tin or silver additions on the ultimate tensile strength (UTS) and the creep-to-failure-time of (i) cast, (ii) rolled, (iii) cast and annealed samples. These experiments confirm the beneficial effect of tin and silver additions on the mechanical properties of Pb–Ca–Sn–Al alloys.

In summary, it could be said that an alloy containing

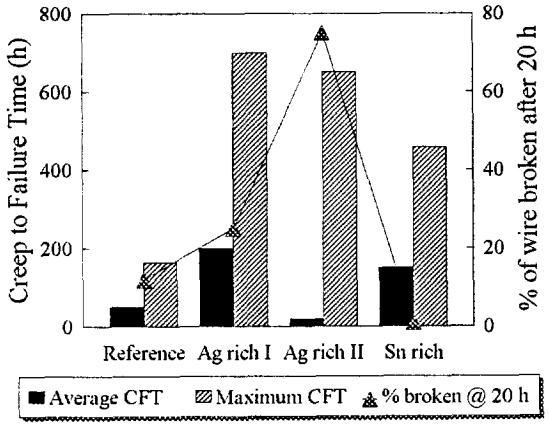

Fig. 4. Creep resistance of grid wires at 27 MPa.

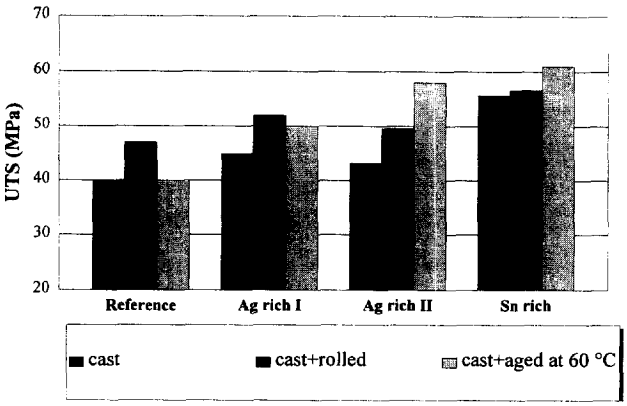

Fig. 5. Ultimate tensile strength (UTS) Pb–0.08wt.%Ca–0.6wt.%Sn samples aged for 72 h at 60 °C.

1.2 wt.% Sn or 0.6 wt.% Sn and 0.05 wt.% Ag is technically compatible with the alloy process and the grid manufacturing and increases significantly the mechanical properties of cast and rolled alloys. It has also been demonstrated that a silver addition to a level of 0.1 wt.% has a delaying effect on the occurrence of the 'overageing' phenomenon but is not compatible with the grid-manufacturing process due to the brittleness of the alloy.

3.2. Corrosion resistance of silver-rich and tin-rich alloys

The corrosion resistance, under +1500 mV, of Pb–Ca–Sn alloys with or without tin and silver is represented by the weight loss versus composition graph given in Fig. 7. This clearly indicates that: (i) calcium-rich (0.1 wt.%) alloys are more sensitive to corrosion than calcium-poor (0.08 wt.%) alloys; (ii) the weight loss passes through a maximum when the tin composition is around 0.6 wt.%; (iii) the weight loss decreases to the level of a tin-free alloy when the amount of tin exceeds 1 wt.%, and (iv) a silver addition, for a given percentage of tin and calcium, has a beneficial effect of the corrosion resistance of the alloy.

The microstructure of one of these samples after the

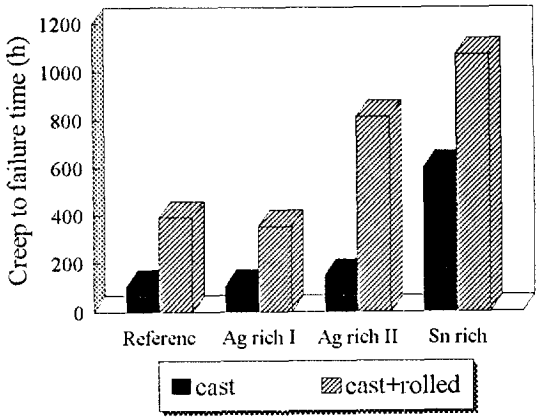

Fig. 6. Creep resistance of Pb–0.08wt.%Ca–0.6wt.%Sn at 20.7 MPa, samples aged for 72 h at 60 °C.

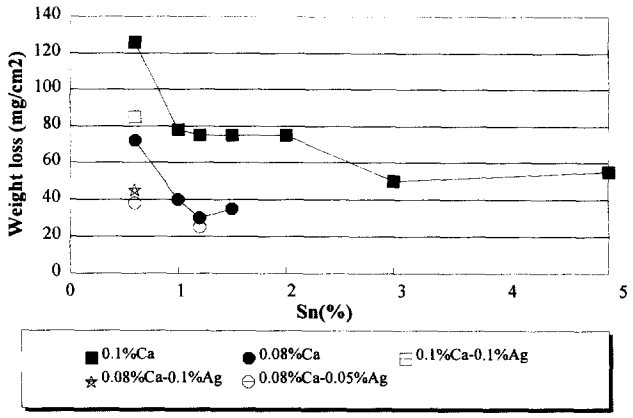

Fig. 7. Amount of corrosion products formed after 5 days at 1500 mV in 5 M H_2SO_4 at 50 °C.

removal of the corrosion products is shown in Fig. 8. It can be seen that the corrosion occurs preferentially in the overaged areas.

Further investigations carried out on bare grids polarized for 13 days at +1500 mV in 5 M H_2SO_4 show that for the reference alloy the corrosion occurs preferentially at the grain boundaries. The beneficial effect of silver is demonstrated by the regularity of the corrosion attack which is dramatically improved with the silver addition (Fig. 9).

Since no significant improvement was recorded when the silver addition was increased up to 0.1 wt.%, it can be concluded that the 0.05 wt.% addition is sufficient to provide the protecting effect.

In summary, it can be said that both tin and silver additions increase the corrosion resistance of Pb–Ca–Sn alloys and that the phenomenon becomes significant when the silver and tin content exceeds, respectively, 0.05 and 1 wt.%.

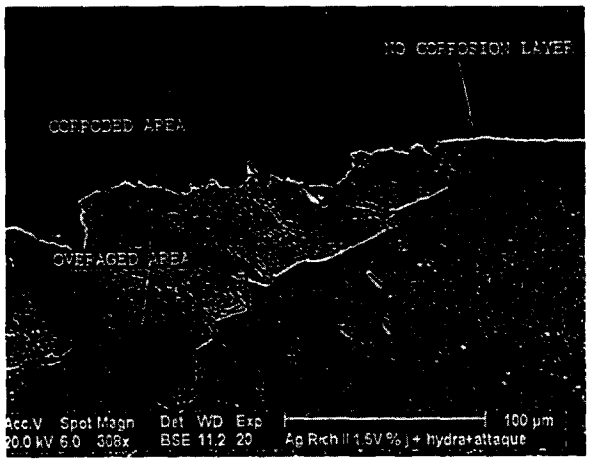

Fig. 8. Sensitivity of the overaged areas to the corrosion phenomenon after 5 days at 1500 mV.

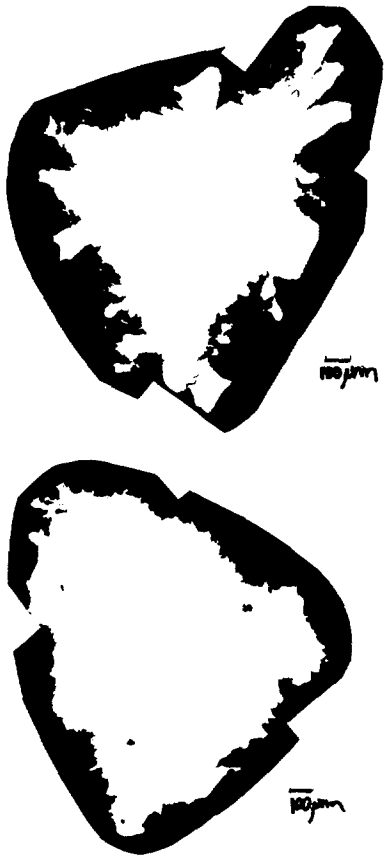

Fig. 9. Cross sections of corroded bare grids after 13 days at 1500 mV in 4.8 M H_2SO_4 at 25 °C.

3.3. Passivation resistance of silver-rich and tin-rich alloys

The passivation resistance of Pb–Ca–Sn bare grids enriched, or not, with tin and silver was evaluated by a voltammetric method using the two criteria R and C. The R and C criteria are close to unity when the conductivity of the corrosion products formed at the metal surface after a polarization period at 700 mV is improved. Tin and silver improve the passivation resistance of bare grids (Table 2).

This result is consistent with the observations carried out on cross sections of laboratory samples polarized at 700 mV. This type of corrosion gives rise to the growth of

Table 2
Passivation test on bare grids: characteristics after 18 h at 700 mV in 0.3 M H_2SO_4

Alloy	R	C
Reference	2.0	1.8
Sn-rich	1.2	0.7
Ag-rich I	1.6	1.4
Ag-rich II	1.7	1.5

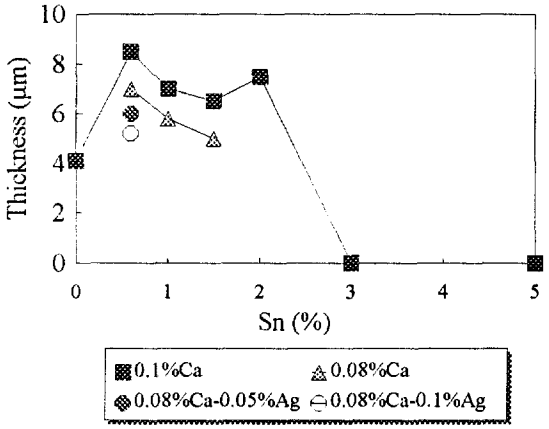

Fig. 10. Thickness of the PbO layer after 7 days at 700 mV in 0.5 M H_2SO_4 at 20 °C.

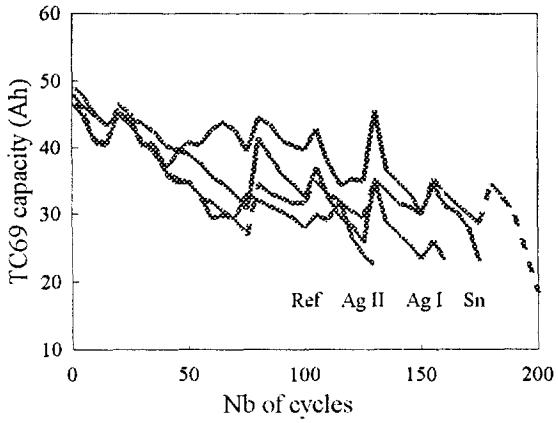

Fig. 12. TC 69 capacity vs. cycle number.

a duplex coating with a thin (2 μm) and porous $PbSO_4$ layer covering a thicker layer of PbO.

The thickness of the $PbSO_4$ layer is found to be independent on the alloy composition, while the thickness of the PbO layer (Fig. 10) is strongly dependent on the tin content. Up to a level of 2 wt.% Sn, the thickness of the PbO layer decreases slightly with the amount of tin but sharply when the tin content exceeds 2 wt.%. With a tin content of 3 wt.%, the PbO layer cannot even be detected.

Microprobe investigations suggest that tin is present in the PbO layer and that the tin distribution is closely related to the alloy composition (Fig. 11).

The presence of tin in the PbO layer has been indirectly confirmed by Vickers measurements on samples that contain 0.1 wt.% of calcium that show the microhardness of the PbO layer to increase (from 100 Hv with 0 wt.% Sn to 170 Hv with 0.6 wt.%Sn and 230 Hv with 1.5 wt.%Sn) with the amount of tin in the alloy.

For a given (0.6 wt.%) amount of tin, the effect of silver addition on the properties of the corrosion layer can be described as follows:

(i) it induces a small decrease (Fig. 10 from 7 μm with 0 wt.% Ag to 5 μm with 0.1 wt.% Ag) in the thickness of the PbO layer, perhaps due to the substitution in the oxide lattice of monovalent silver for lead;

(ii) it contributes to the growth of a harder (from 170 Hv with 0 wt.%Ag to 270 Hv with 0.1 wt.%Ag) layer, and

(iii) it improves the regularity of the PbO layer formed at the metal surface.

In summary, it can be said that tin and silver additions to the alloy modify the characteristics of the PbO layer formed at the metal surface. Tin decreases (for a tin content of 3 wt.%) the thickness of the PbO layer and increases, as demonstrated by voltammetric scans, the conductivity of the corrosion products formed under conditions that simulate a deep discharge. These results are in good agreement with the published literature [4–6].

3.4. Battery performance

Figs. 12 and 13 display, respectively, the evolution of the TC 69 capacity and the $C/5$ capacity, during a TC 69 cycling test with 100% depth-of-discharge, as a function of cycle number. This clearly indicates that the batteries using the tin-rich and silver-rich I alloys retain the highest

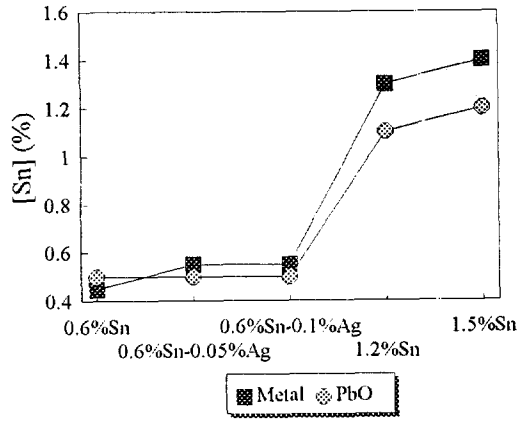

Fig. 11. Tin distribution between metal and PbO after 7 days at 700 mV in 0.5 M H_2SO_4.

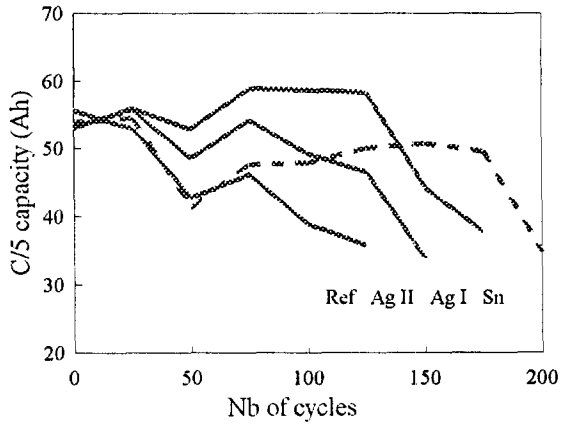

Fig. 13. C/5 capacity vs. cycle number.

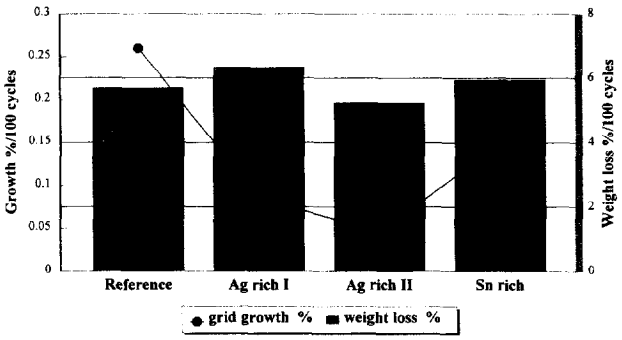

Fig. 14. Postmortem analysis: grid growth and weight loss after cycling.

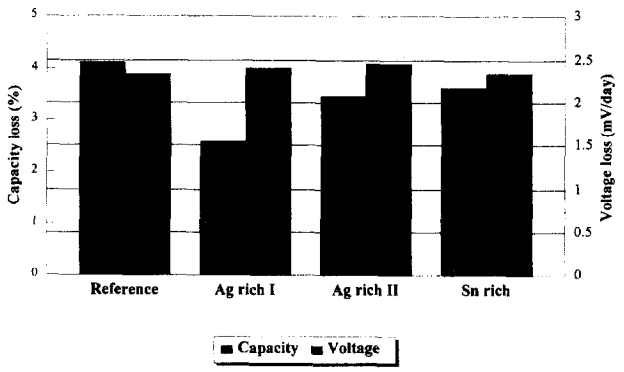

Fig. 16. Self-discharge behaviour after 90 days at 25 °C.

capacity and the longest cycle life upon deep cycling, compared with the reference alloy which displays an early failure after only 125 cycles under the severe conditions.

After cycling, all the batteries were dismantled for tear-down analysis. The measurement of the grid dimensions showed that the grid growth phenomenon was negligible since, as seen in Fig. 14, all the variations were lower than 0.4%. The weight variation of the grids after dissolution of the corrosion products formed at the metal surface during cycling (Fig. 14) indicates that the degree of corrosion of the tin-rich alloy may be slightly higher than that of the reference alloy but, again, the differences are not really significant. These results suggest, therefore, that the batteries did not die from failure of the positive grids, but rather from a phenomenon at the grid/active-material interface or from a softening problem of the positive active mass.

The negative active mass was subjected to chemical analysis by atomic absorption spectroscopy. The negative material displayed, after cycling, significant enrichment in tin and silver that was closely related to the alloy composition, thus suggesting that both silver (as Ag^{+}) and tin (as Sn^{2+} or Sn^{4+}) had migrated from the positive grid to the negative material (see Fig. 15). This may also have an effect on the self-discharge and the water consumption as silver is known to decrease the O_2 and H_2 overvoltages and facilitate electrolyte decomposition. Although, measurable, this effect was rather low since, as shown in Fig. 15,

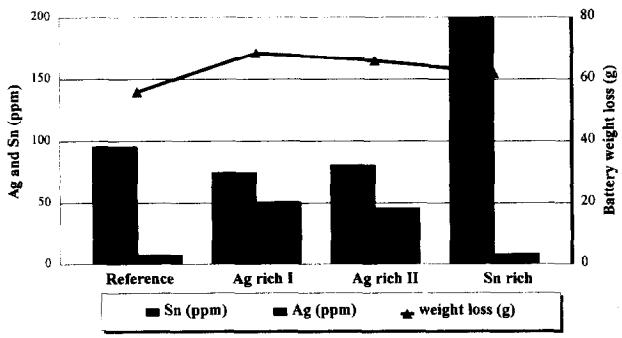

Fig. 15. Postmortem analysis: negative active mass analysis and battery weight loss after cycling.

the weight variation of the batteries is independent of the positive-grid composition.

The capacity loss (in %) and the voltage loss (in mV/day) after 90 days of storage at 25 °C and open circuit are given in Fig. 16. The highest capacity loss was observed on the reference batteries, while the lowest was measured on the batteries containing the silver-rich I alloy. The decrease in the battery voltage was similar for both the silver-free batteries, but was greater when the silver content was increased.

4. Discussion

The evolution of microstructures and mechanical properties depend on the tin/calcium weight ratio [2,7,8]. After rapid cooling of the lead alloy, the α-Pb matrix is oversaturated and suitable for the formation of precipitates of calcium compounds.

With a tin/calcium ratio of around 7 (i.e., for the reference alloy with 0.08 wt.% Ca and 0.6 wt.% Sn), a Pb–Ca–Sn alloy exhibits four (often incomplete) transformations namely:

(i) a linear, discontinuous, transformation immediately after cooling;

(ii) a second transformation with an irregular motion of grain boundaries, called 'puzzling', that is generally achieved after 24 h;

(iii) a continuous bulk precipitation of the $(Pb_{1-x}Sn_x)_3Ca$ phase, with the $L1_2$ structure, which takes place after an incubation period, and

(iv) a discontinuous transformation related to the reaction $[(Pb_{1-x}Sn_x)_3Ca]_{\text{finally dispersed precipitates}} \rightarrow [(Pb_{1-x}Sn_x)_3Ca]_{\text{large lamellar precipitates}}$ (overaging phenomenon).

With a tin/calcium ratio of around 15 (i.e., a tin-rich alloy with 0.08 wt.% Ca and 1.2 wt.% Sn), only two types of transformation can been observed: (i) a continuous bulk precipitation of the $(Pb_{1-x}Sn_x)_3Ca$ phase, and (ii) the overageing reaction.

The observations made on the reference alloy (puzzling and overageing phenomena) and the tin-rich alloy (conservation of the foundry structure and overageing phenomon) are in good agreement with the published literature [2,7,8].

With silver addition, the solidification of the α-Pb phase induces the segregation of silver-based compounds. According to the binary phase diagrams, the compounds that can be formed are: metallic Al, metallic Sn and the intermetallics Ag_3Sn, Ag_2Ca and Ag_2Al_3. Upon ageing, the oversaturated α-Pb matrix will evolute, depending on the tin/calcium ratio, while the segregations at grain boundaries will be probably stable. The presence of these segregated elements may inhibit the formation of large $[(Pb_{1-x}Sn_x)_3Ca]$ precipitates by preventing the diffusion then the coalescence of the fine $[(Pb_{1-x}Sn_x)_3Ca]$ precipitates and could, therefore, provide an explanation of the delaying effect of silver on the occurrence of the overageing phenomenon. This mechanism could explain the good mechanical properties observed for silver-rich alloys.

The delay of the overageing phenomonenon has also an important effect on the corrosion resistance at +1500 mV. The observed improvements may be due to a better accommodation of stresses induced by the corrosion layer growth in the non-overaged areas where the mechanical properties are superior. The finer distribution of precipitates of $(Pb_{1-x}Sn_x)_3Ca$ in these areas may also promote very uniform corrosion.

Concerning the role of tin, this study confirms that this element increases the conductivity of the corrosion layer and, more particulary, of the α-PbO oxide that develops under deep-discharge conditions [9]. For amounts of tin less than 2 wt.%, the PbO is present under a superficial layer of $PbSO_4$ and the improvement in the conductivity may be attributed to the presence of SnO_2 precipitated at the grain boundaries [10] of the lead monoxide. For an upper level that corresponds to the presence of free tin in a three-phase alloy, the sulfate layer is more porous and the growth of the PbO layer is inhibited.

If the set of experiments conducted on a laboratory (evaluation of mechanical properties, passivation resistance at +700 mV and corrosion resistance at +1500 mV) was a pre-requisite for the definition of a Pb–Ca–Sn alloy, this work needed to be completed by experiments carried out on fully operative batteries. These experiments do not really provide a check of the properties (improvements in the mechanical properties and the corrosion resistance of the alloys) claimed during the laboratory-scale experiments since, as depicted by the tear-down analysis, the batteries did not die from grid failure but rather from a softening of the positive active mass. A reason for such a behavior could be the severity of the cycling test (TC 69 with 100% depth-of-discharge instead of 80%) adopted in this study.

Nevertheless, the experiments have demonstrated that the alloy composition has a dramatic impact on the performance of the batteries since the number of cycles achieved are closely related to the alloy composition. They have also shown that silver addition, at a level of 0.05 wt.%, has no perceptible effect, as initially feared, on the self-discharge at room temperature and the gassing behaviour of the batteries.

For the development of a lead/acid battery for EV applications, the use of an alloy containing 1.2 wt.% Sn and 0.05 wt.% Ag is proposed for the positive grid. The improvement in the mechanical properties with both tin and silver additions would enable the processing of thinner (2 mm) grids with a better corrosion resistance due to the silver addition and an improved passivation resistance due to the presence of tin. As observed during TC 69 tests, the batteries should also benefit from a longer cycle life and a better rechargeability.

The addition of tin and silver to the alloy would enable manufacturers to reduce the grid/active-material weight ratio and, therefore provide a significant improvement in the specific power and specific energy without sacrificing cycle life. The use of a Pb–Ca–Sn–Ag alloy would help the battery manufacturers to reach the ALABC's target density of 50 Wh kg^{-1}.

5. Conclusions

The objective of this research programme is to develop and test, under industrial conditions, an alloy for the positive grid with improved mechanical, corrosion resistance and passivation resistance properties. The following results have been obtained.

1. Tin (at a level of 1.2 wt.%) and silver (at a level of 0.05 wt.%) significantly increase the mechanical properties of Pb–Ca–Sn alloys.

2. Silver (at a level of 0.1 wt.%) exerts a delaying effect on the occurrence of the 'overageing' phenomenon.

3. Tin (at a level of 1.2 wt.%) reduces the passivation of Pb–Ca–Sn alloys under conditions that simulate a deep-discharge by increasing the conductivity of the PbO layer formed at the metal surface.

4. Silver (at a level of 0.05 wt.%) increases the corrosion resistance of Pb–Ca–Sn alloys under conditions that simulate the end-of-charge.

5. Tin (at a level of 1.2 wt.%) and silver (at a level of 0.05 wt.%) additions in the positive grid improve the cycle life and the capacity of lead/acid batteries.

6. Tin (at a level of 1.2 wt.%) and silver (at a level of 0.05 wt.%) additions in the alloy exert a limited effect on the battery behaviour under self-discharge conditions at room temperature.

7. Tin-rich and silver-rich alloys, with the exception of the silver-rich II (0.1 wt.%) alloy, can be introduced directly in the cast shop for the processing of positive grids for EV batteries.

Acknowledgements

The authors are grateful to the European Union and the Advanced Lead–Acid Battery Consortium for providing support for this study within the framework of the Brite Euram II EALABC program.

References

[1] R. Miraglio, L. Albert, A. El Ghachcham, J. Steinmetz and J.P. Hilger, *J. Power Sources, 53* (1995) 53.
[2] L. Bouirden, J.P. Hilger and J. Hertz, *J. Power Sources, 33* (1991) 27–50.
[3] H. Giess, *J. Power Sources, 53* (1995) 31–43.
[4] H.K. Giess, in K.R. Bullock and D. Pavlov (eds.), *Proc. Symp. Advances in Lead–Acid Batteries*, Proc. Vol. 84-14, The Electrochemical Society, Pennington NJ, USA, 1984, p. 241.
[5] D. Pavlov, B. Monakhov, M. Maja and N. Penazzi, *J. Electrochem. Soc., 136* (1989) 27.
[6] M.N.C. Ijomah, *J. Electrochem. Soc., 134* (1987) 2960.
[7] J.P. Hilger, *Structural Transformation in Lead Alloys, Short Intensive Training Course*, COMETT, Nancy, France, 25–26 Mar. 1993.
[8] J.P. Hilger and L. Bouirden, *J. Alloys Comp., 236* (1996) 224–228.
[9] P. Mattesco, N. Bui, P. Simon and L. Albert, *J. Power Sources, 64* (1997) 21–27.
[10] A. El Ghachcham Amrani, Ph. Steyer, J. Steinmetz, P. Delcroix and G. Le Caer, *J. Power Sources, 64* (1997) 35–37.
[11] G.-L. Wei and J.-R. Wang, *J. Power Sources, 52* (1994) 81–85.